Electronic Supplementary Information

Accelerating the oxygen evolution reaction kinetics of Co_3O_4 in neutral electrolyte by decorating RuO_2

Kaifa Lu,[a]† Guanru Chang,[abc]† Hui Zhang*[a] and Xin-Yao Yu*[bde]

[a]School of Physics and Materials Science, Anhui University, Hefei 230601, P. R. China. Email: zhhui@ahu.edu.cn

[b]Institutes of Physical Science and Information Technology, Key Laboratory of Structure and Functional Regulation of Hybrid Materials, Anhui University, Ministry of Education, Hefei 230601, P. R. China. E-mail: yuxinyao@ahu.edu.cn

[c]School of Chemistry and Chemical Engineering, Huangshan University, Huangshan 245041, P. R. China
[d]Anhui Graphene Engineering Laboratory, Anhui University, Hefei 230601, P. R. China

[e]Energy Materials and Devices Key Lab of Anhui Province for Photoelectric Conversion, Anhui University, Hefei 230601, P. R. China

†*These two authors contribute equally to this work*

Experimental Section

Synthesis of CCH and Ru_x-CCH

Nickel foam (NF) (2×3 cm^2) was first rinsed in 3 M hydrochloric acid for 10 min and then sonicated in ethanol and deionized water for 10 min in succession. In a typical process for the synthesis of cobalt carbonate hydroxide (CCH) nanorod arrays, 5 mmol of Co $(NO_3)_2$ and 25 mmol of urea were first dissolved in 40 ml of deionized water and the solution was transferred into a 50 ml Teflon-lined stainless-steel reactor. Then, the NF was put into the autoclave and the autoclave was subsequently put into the oven and heated at 90 ^oC for 7 h. After the hydrothermal reaction is finished, the sample is taken out and washed and dried for use. The synthesis of Ru_x-CCH is similar to that of CCH except adding 0.05, 0.15, and 0.25 mmol of $RuCl_3$. The samples obtained with addition of 0.05, 0.15, and 0.25 mmol of $RuCl_3$ were named as Ru_1-CCH, Ru-CCH, and Ru_2-CCH, respectively.

Synthesis of Co_3O_4, RuO_2/Co_3O_4-1, RuO_2/Co_3O_4, and RuO_2/Co_3O_4-2

The as-synthesized CCH and Ru_x-CCH were put in a muffle furnace and heated at 350 ^oC in air for 3 h at a heating rate of 5 ^oC per minute. The corresponding metal oxides named as Co_3O_4, RuO_2/Co_3O_4-1, RuO_2/Co_3O_4, and RuO_2/Co_3O_4-2 were obtained by calcination of CCH, Ru_1-CCH, Ru-CCH, and Ru_2-CCH, respectively. The loading of catalysts on the surface of Ni foam were calculated by weighting the mass change of Ni foam before and after catalysts growth. The loading of Co_3O_4, RuO_2/Co_3O_4-1, RuO_2/Co_3O_4, and RuO_2/Co_3O_4-2 is around 1200 μg cm^{-2}. The loading of RuO_2 was then calculated by XPS analysis and was determined to be 54, 146, and 228 μg cm^{-2} for RuO_2/Co_3O_4-1, RuO_2/Co_3O_4, and RuO_2/Co_3O_4-2, respectively.

Material Characterizations

X-ray diffraction (XRD) data were measured by the X-ray diffractometer (DX-2700). The morphology of the sample was observed with Hitachi S4800 scanning electron microscope (SEM). Raman spectra were collected on a Via-Reflex Raman microscope equipped with a 532 nm laser. A FEI tecnai G2F20 S-Twin instrument was used to obtain the transmission electron microscope (TEM) image, elemental mapping images and the electron diffraction pattern of the selected area. X-ray photoelectron spectroscopy (XPS) and ultraviolet photoelectron spectroscopy (UPS) were performed on ESCALAB-MKII spectrometer (VG Company, UK). The work function of the material is calculated according to the positions of the secondary electron cut-off edge and the Fermi edge of the UPS spectrum. E_{Fermi} is the abscissa value corresponding to the intersection of the tangent line of the Fermi edge and the baseline, and E_{Cutoff} corresponds to the abscissa value of the midpoint of the secondary electron cut-off edge curve.[1,2] The work function can be estimated according to the following formula[3]:

$$h\nu - \Phi = E_{Fermi} - E_{Cutoff}$$

$$\Phi = h\nu + E_{Cutoff} - E_{Fermi}$$

Where $h\nu$ is the known excitation energy and Φ represents work function.

Electrochemical characterizations

Electrochemical tests were carried out on CHI electrochemical workstation and

Biologic multi-channel potentiostat. Under the standard three-electrode system, the NF with the growth of catalysts (geometric area: 0.5 cm^{-2}) was used as the working electrode, the carbon rod was used as counter electrode, and Ag/AgCl was employed as reference electrode. 1 M phosphate buffer solution (PBS) with a pH of 7 was used as the electrolyte. Before the OER performance test, dozens of voltammetry cycles were carried out or *I-t* test at 10 mA cm^{-2} on the sample until the performance of the material was stable. The range of the voltammetry cycles was 1.1-1.9 V *vs*. RHE at a scan rate of 50 mV s^{-1}. The linear sweep voltammetry curves were tested in the range of 1.1-1.9 V *vs*. RHE at a scan speed of 5 mV s^{-1}. All the LSV curves were i*R* corrected. 85% i*R* correction was applied manually to all the as-recorded LSV curves based on the resistance (R_{OCP}) at open circuit potential. $0.85 \times i \times R_{OCP}$ was subtracted from the recorded voltage values in the LSV to apply the correction. Conversion relationship between reversible hydrogen electrode and Ag/AgCl electrode is as follows:

$$E_{RHE} = E_{exp} + E_{Ag/AgCl} + 0.059 \times pH$$

Faraday efficiency was calculated by the rotating ring disk electrode (RRDE) test. The RRDE is composed of glassy carbon disk and Pt ring. The catalysts were peeled off from the surface of Ni foam by sonication. Then, 5 mg of the catalysts powders were dispersed into a mixed solution containing 270 μL of ethanol, 200 μL of water, and 30 μL of Nafion solution (5wt%). 2.5 μL of the as-obtained ink was dropped onto the disk electrode. The RRDE ring potential was maintained at 0 V *vs*. RHE to reduce the O_2 produced by the catalyst on the disk electrode. The Faraday efficiency (ε) is calculated according to the following equation:

$$\varepsilon = I_r/(I_d N)$$

Where I_d, I_r and N represents the RRDE disk current, ring current and current collection efficiency (here is 0.424), respectively.

Methods of DFT calculations

We have employed the first-principles[4,5] to perform density functional theory (DFT) calculations within the generalized gradient approximation (GGA) using the Perdew-Burke-Ernzerhof (PBE)[6] formulation. We have chosen the projected augmented wave (PAW) potentials[7,8] to describe the ionic cores and take valence electrons into account using a plane wave basis set with a kinetic energy cutoff of 400 eV. Partial occupancies of the Kohn-Sham orbitals were allowed using the Gaussian smearing method and a width of 0.05 eV. The 3×3×1 *k*-points has been chosen, and the electronic energy was considered self-consistent when the energy change was smaller than 10^{-6} eV. A geometry optimization was considered convergent when the energy change was smaller than 0.05 eV $Å^{-1}$. In addition, for the Co atoms, the *U* schemes need to be applied, and the *U* has been set as 3.1 eV. The spin correction has been employed to describe the electronic properties. The reaction free energies were calculated using the equation:

$$G = E + ZPE - TS$$

Where *G*, *E*, *ZPE* and *TS* are the free energy, total energy from DFT calculations, zero-point energy, and entropic contributions, respectively.

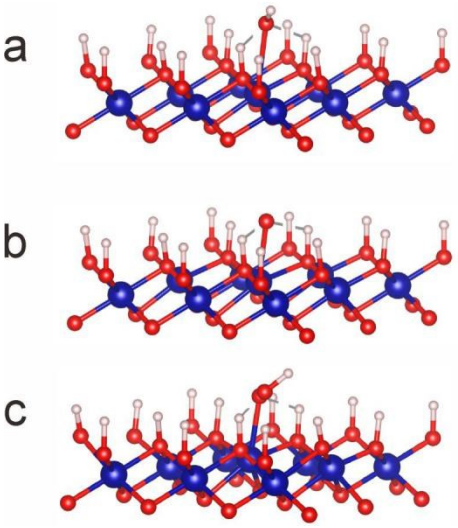

Fig. S1 Adsorption configuration of (a) OH*, (b) O*, and (c) OOH* on CoOOH. The blue, red, and white balls represent Co, O, and H atoms, respectively.

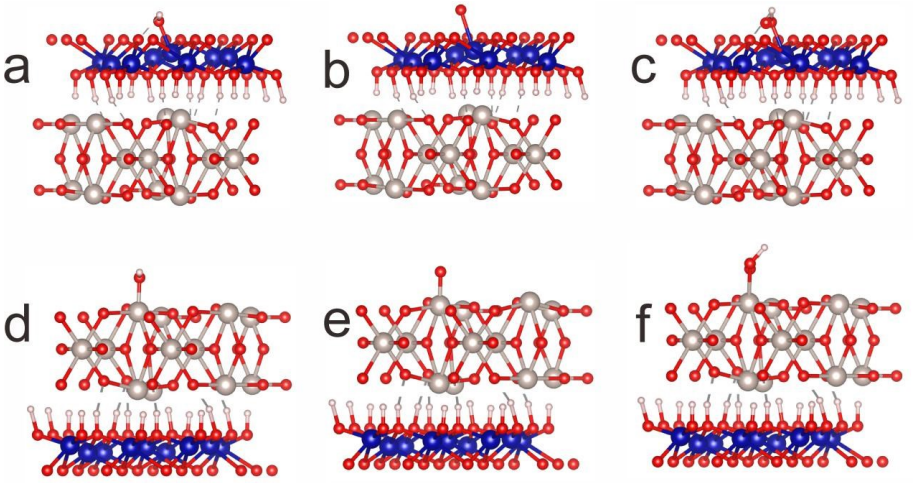

Fig. S2 Adsorption configuration of (a) OH*, (b) O*, and (c) OOH* on Co site of RuO_2/CoOOH; Adsorption configuration of (d) OH*, (e) O*, and (f) OOH* on Ru site of RuO_2/CoOOH. The blue, gray, red, and white balls represent Co, Ru, O, and H atoms, respectively.

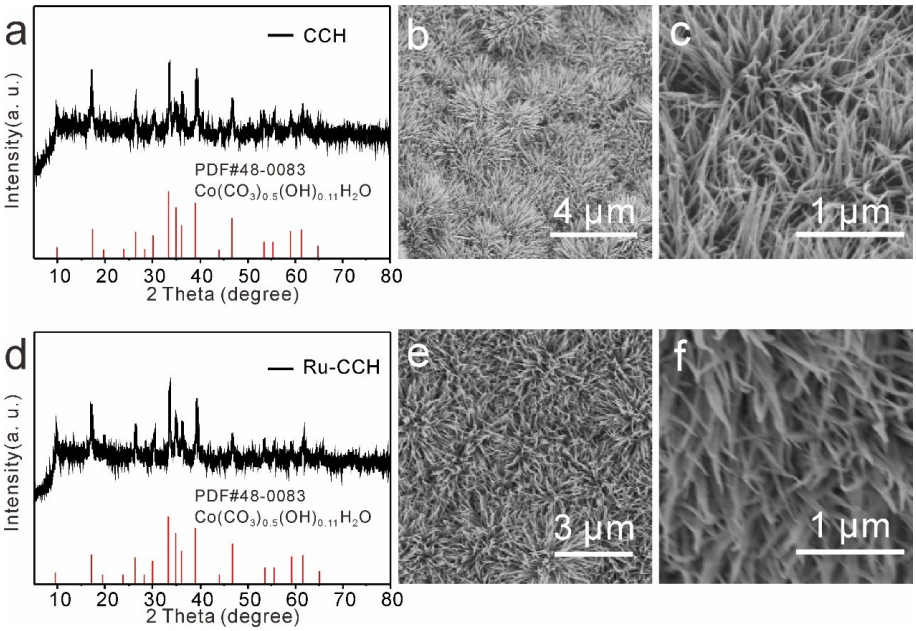

Fig. S3 (a,b) XRD patterns and (b,c,e,f) SEM images of CCH (a,b,c) and Ru-CCH (d,e,f).

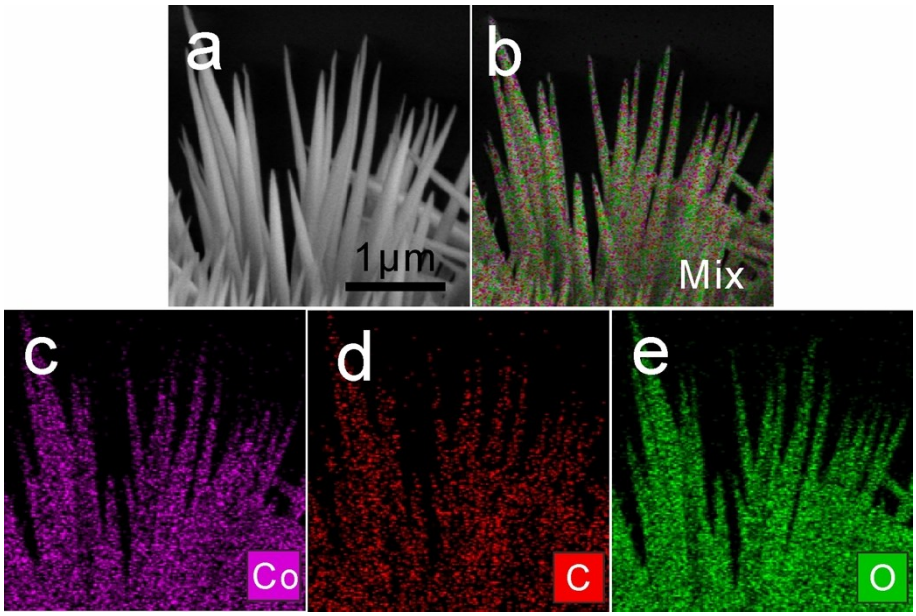

Fig. S4 (a) SEM image and (b-e) corresponding EDX elemental mapping images of CCH.

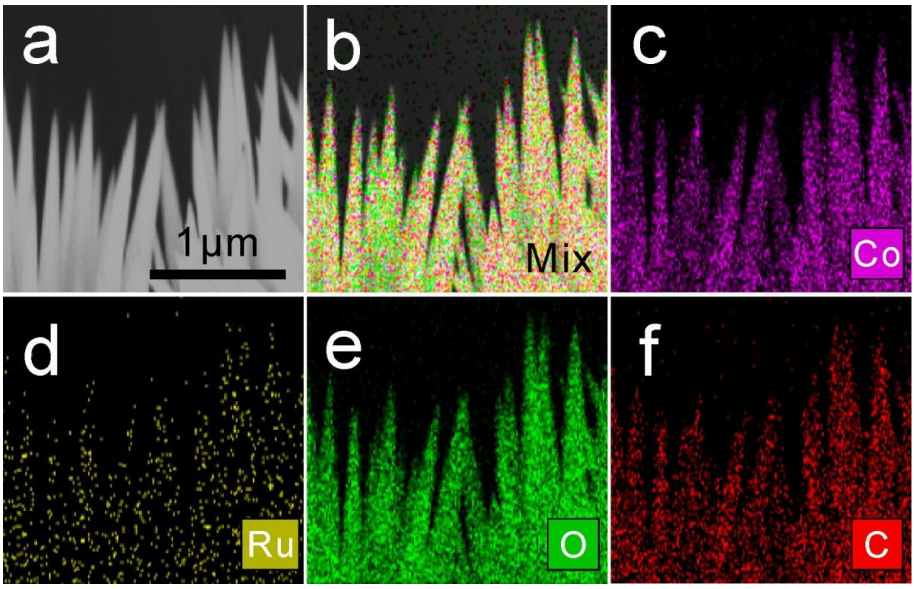

Fig. S5 (a) SEM image and (b-f) corresponding EDX elemental mapping images of Ru-CCH.

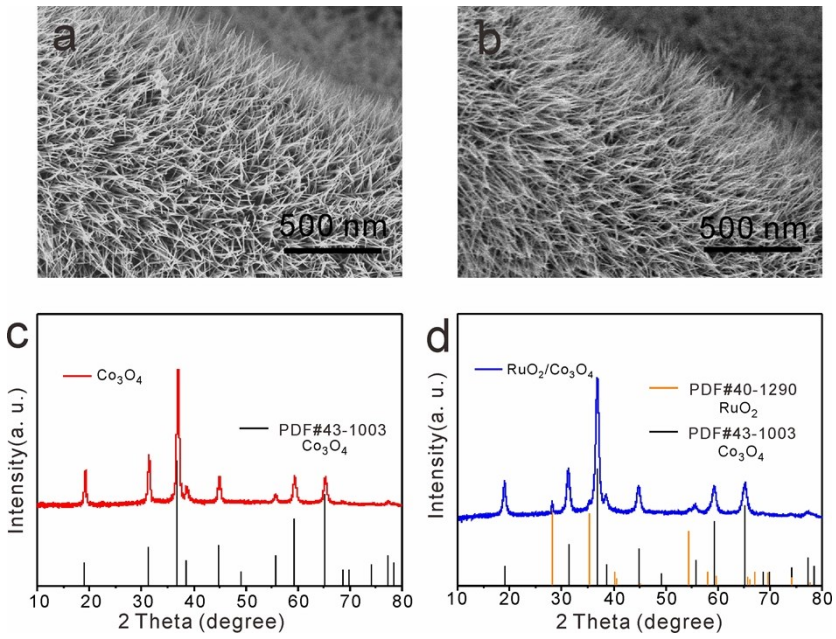

Fig. S6 (a,b) Large-scale SEM images and (c,d) XRD patterns of Co_3O_4 (a,c) and RuO_2/Co_3O_4 (b,d) nanorod arrays.

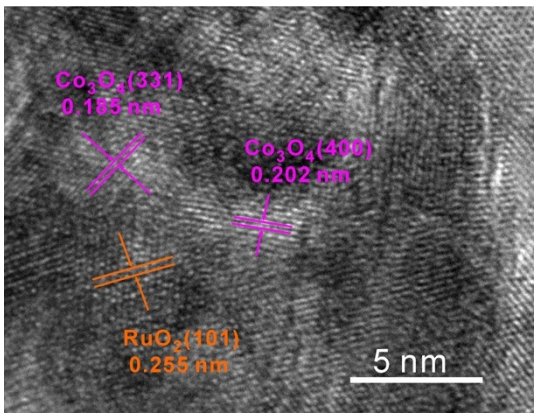

Fig. S7 HRTEM image of RuO_2/Co_3O_4 nanorod.

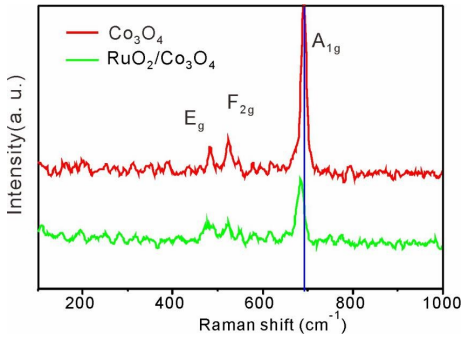

Fig. S8 Raman spectra of Co_3O_4 and RuO_2/Co_3O_4 nanorod arrays.

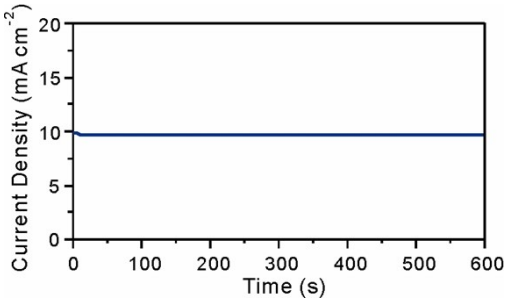

Fig. S9 *I-t* curve of RuO_2/Co_3O_4 nanorod arrays at 10 mA cm^{-2} before LSV test.

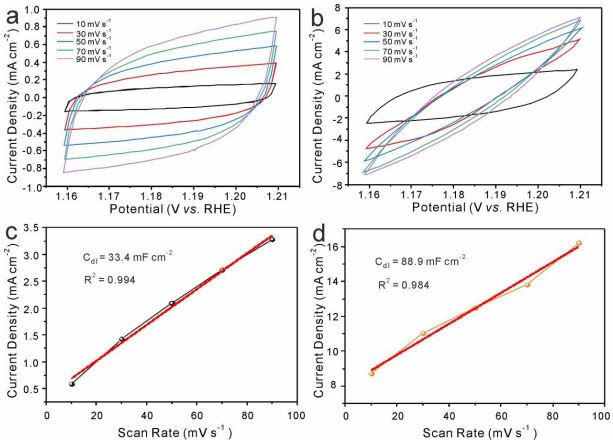

Fig. S10 (a,b) CV curves at different scanning rates in the non-Faraday region and (c,d) plots for C_{dl} calculation of Co_3O_4 and RuO_2/Co_3O_4 nanorod arrays.

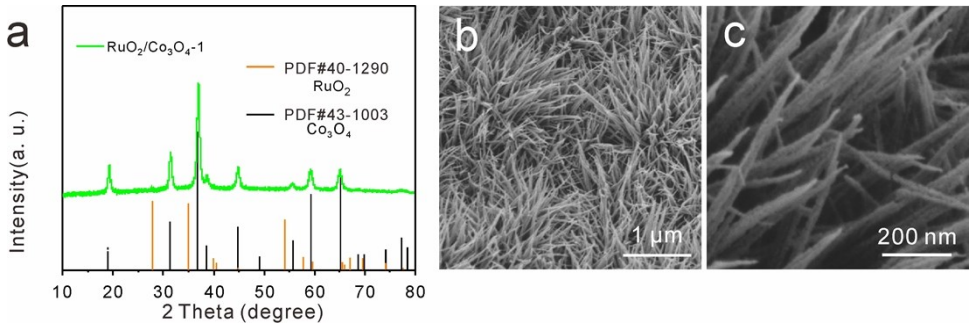

Fig. S11 (a) XRD pattern and (b,c) SEM images of RuO_2/Co_3O_4-1 nanorod arrays.

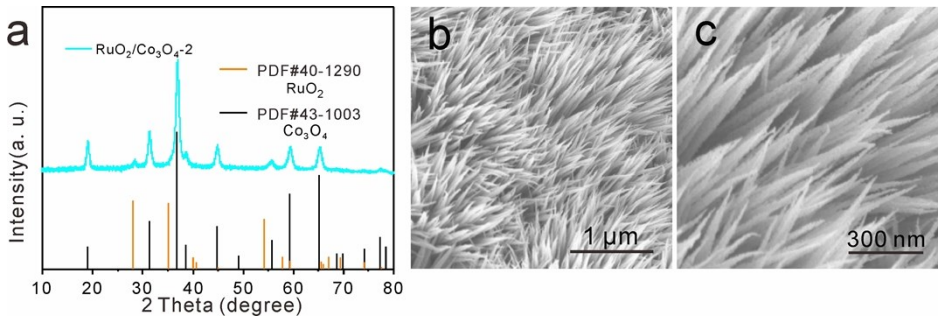

Fig. S12 (a) XRD pattern and (b,c) SEM images of RuO_2/Co_3O_4-2 nanorod arrays.

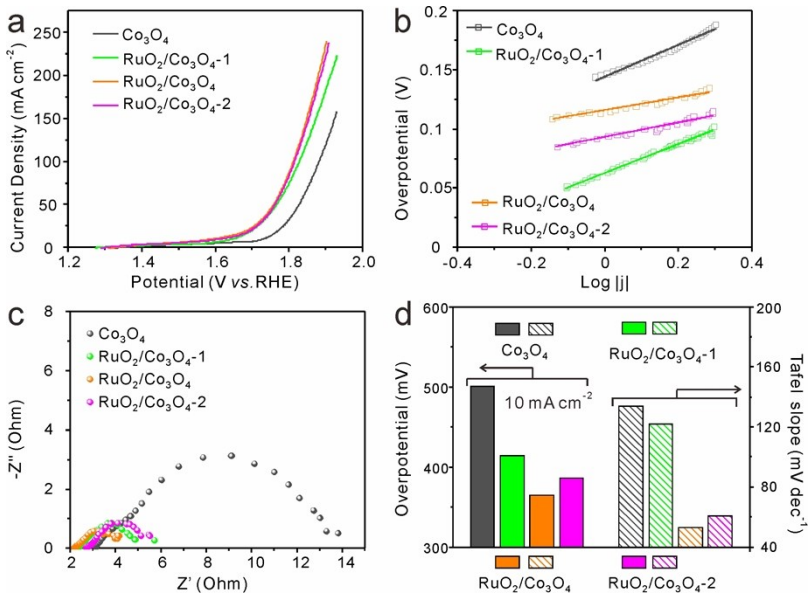

Fig. S13 (a) LSV curves, (b) Tafel plots, and (c) Nyquist plots of Co_3O_4, RuO_2/Co_3O_4-1, RuO_2/Co_3O_4, and RuO_2/Co_3O_4-2 nanorod arrays in 1 M PBS; (d) Overpotentials at 10 mA cm^{-2} and Tafel slopes of Co_3O_4, RuO_2/Co_3O_4-1, RuO_2/Co_3O_4, and RuO_2/Co_3O_4-2 nanorod arrays.

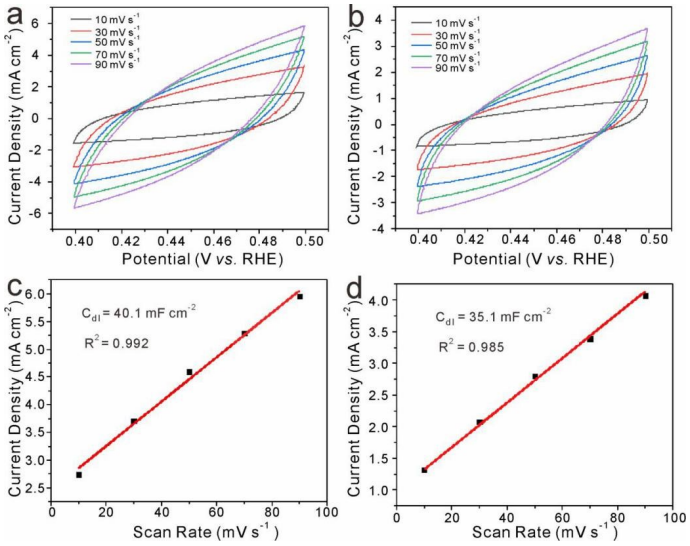

Fig. S14 (a, b) CV curves at different scanning rates in the non-Faraday region and (c, d) plots for C_{dl} calculation of RuO_2/Co_3O_4-1 and RuO_2/Co_3O_4-2 nanorod arrays.

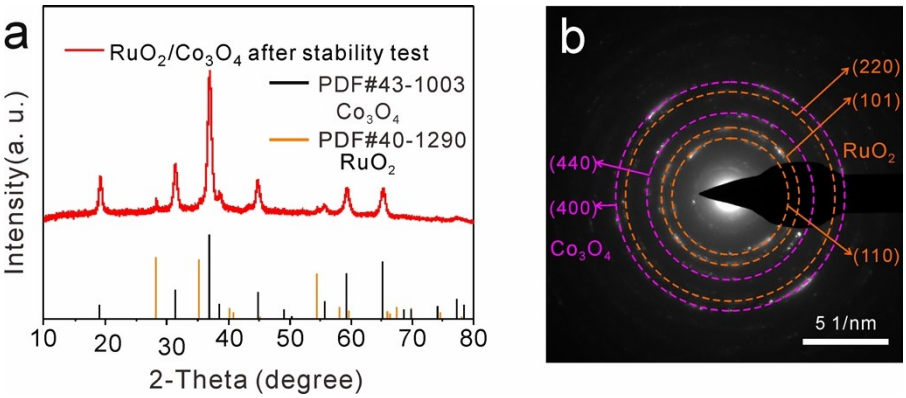

Fig. S15 (a) XRD pattern and (b) SAED pattern of RuO_2/Co_3O_4 nanorod arrays after OER stability test.

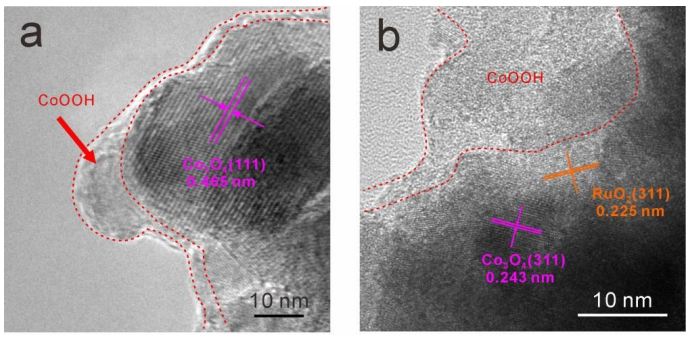

Fig. S16 HRTEM images of (a) Co_3O_4 and (b) RuO_2/Co_3O_4 nanorod arrays after OER stability test.

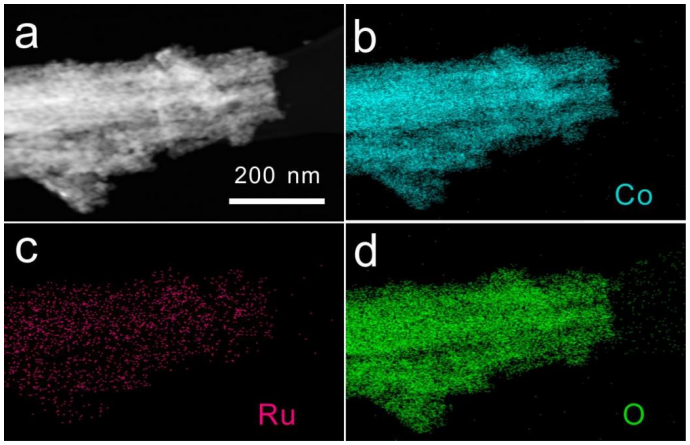

Fig. S17 (a) Scanning TEM image and (b) corresponding EDX elemental mapping images of RuO_2/Co_3O_4 nanorod arrays after OER stability test.

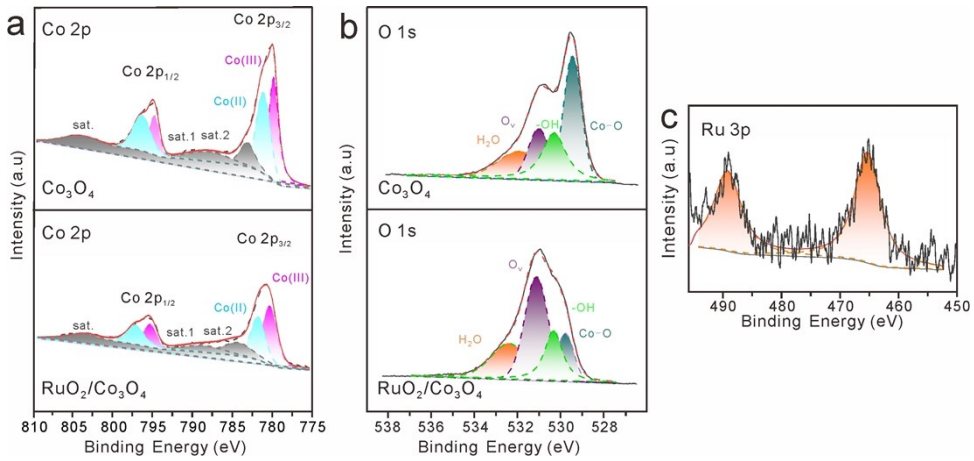

Fig. S18 (a) Co 2p and (b) O 1s high-resolution XPS spectra of Co_3O_4 and RuO_2/Co_3O_4 nanorod arrays after OER stability test; (c) Ru 3p high-resolution XPS spectra of RuO_2/Co_3O_4 nanorod arrays after OER stability test.

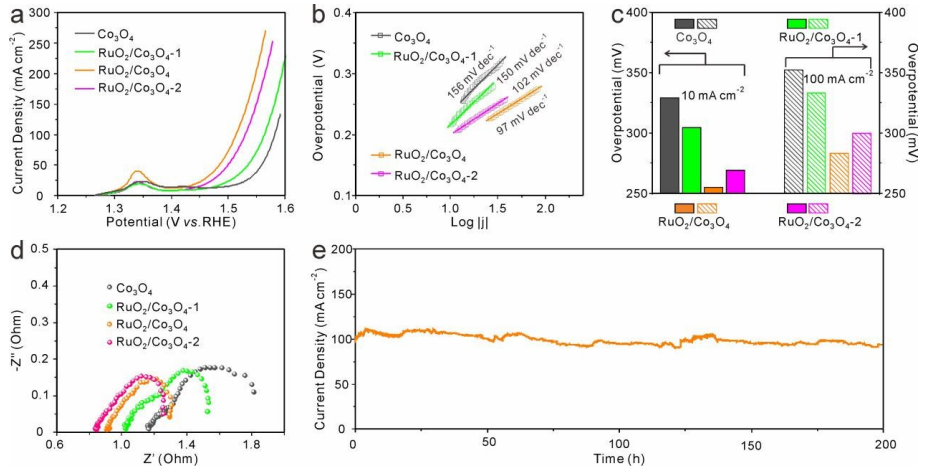

Fig. S19 (a) LSV curves and (b) Tafel plots of Co_3O_4, RuO_2/Co_3O_4-1, RuO_2/Co_3O_4, and RuO_2/Co_3O_4-2 nanorod arrays in 1 M KOH; (c) Overpotentials of Co_3O_4, RuO_2/Co_3O_4-1, RuO_2/Co_3O_4, and RuO_2/Co_3O_4-2 nanorod arrays at 10 and 100 mA cm^{-2}; (d) Nyquist plots of Co_3O_4, RuO_2/Co_3O_4-1, RuO_2/Co_3O_4, and RuO_2/Co_3O_4-2 nanorod arrays; (e) chronoamperometry curve of RuO_2/Co_3O_4 at 100 mA cm^{-2}.

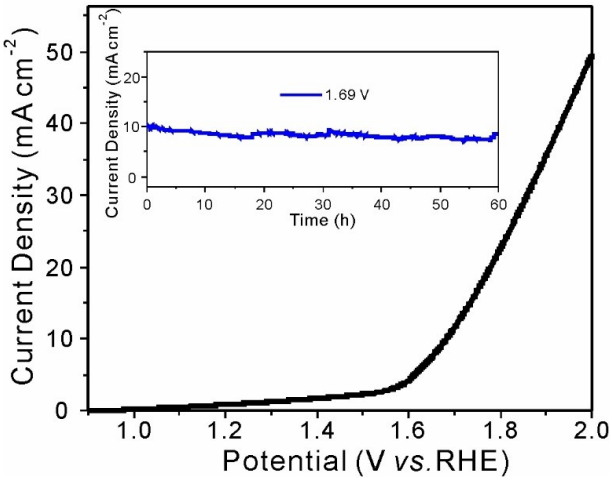

Fig. S20 Polarization curve of full water electrolysis and chronoamperometry curve (inset) of the electrolysis cell by using RuO_2/Co_3O_4 nanorod arrays as anode and commercial Pt/C as cathode in 1 M PBS.

Table S1 Different atomic content measured by the X-ray photoelectron spectroscopy (XPS) survey spectra.

Samples	Ru Atomic %	Co Atomic %	C Atomic %	O Atomic %
Co_3O_4	0	30.16	19.33	49.9
RuO_2/Co_3O_4-1	0.73	28.04	20.3	50.94
RuO_2/Co_3O_4	1.37	18.09	25.12	55.41
RuO_2/Co_3O_4-2	1.85	20.56	24.21	53.39

Table S2 Comparison of OER performance of RuO_2/Co_3O_4 with the most advanced electrocatalyst in neutral electrolytes.

Electrocatalyst	Electrolyte	Overpotential (mV) at 10 mA cm^{-2}	Tafel slope (mV dec^{-1})	Ref.
POM@ZIF-8	0.1 M Na_2SO_4	784.19 (@1 mA cm^{-2})	783.62	9
Co_4-bdt	1 M PBS	430	68	10
Zn,S-CoP NRCs/CP	1 M PBS	391	99.7	11
CeO_2/Co-Bi	0.1 M PBS	453	120	12
CoO_xH_y NSAs	0.1 MPBS	430	121	13
np-Co_9S_8P	1 M PBS	483	106	14
$Na_2CoP_2O_7$	0.5 M PBS	560 (@1 mA cm^{-2})	90	15
SCN-Ru-RuO_2/C_3N_4	1 M PBS	342	92	16
$Co_3(PO_4)_2$@GF	0.1 M PBS	530 (@5 mA cm^{-2})	133	17
Co_3O_4 QDs	0.2 M PBS	490	80	18
$NiCoO_2$@CeO_2 NBs	0.1 M PBS	501 (@1 mA cm^{-2})	72	19
Co_3O_4 /Ti	1 M PBS	544	88	20
$NaCo_4(PO_4)_3$	0.05 M PBS	373 (@1 mA cm^{-2})	121	21
Co-Se-S-O NTs	0.1 M PBS	480	86.1	22
$Co_3(PO_4)_2$	0.1 M PBS	375 (@5 mA cm^{-2})	59	23
$Co_3(BO_3)_2$@CNT	1 M KNO3	487	264	24
RuO_2/Co_3O_4	**1 M PBS**	**365**	**53**	**This work**

Supplementary references

1 J. Sitte, Chem. Phys. Lett., 1976, **42**, 131-132.

2 D. He, X. Song, W. Li, C. Tang, J. Liu, Z. Ke, C. Jiang and X. Xiao, *Angew. Chem. Int. Ed.*, 2020, **132**, 6996-7002.

3 B. Zhang, Y.-Z. Sun, W.-H. Wang, *Phys. Examin. Test.* 2007, **25**, 21- 23.

4 G. Kresse and J. Furthmüller, *Comput. Mater. Sci.*, 1996, **6**, 15-50.

5 G. Kresse and J. Furthmüller, *Phys. Rev. B*, 1996, **54**, 11169.

6 J. P. Perdew, K. Burke and M. Ernzerhof, *Phys. Rev. Lett.*, 1996, **77**, 3865.

7 Kresse and D. Joubert, *Phys. Rev. B*, 1999, **59**, 1758.

8 P. E. Blöchl, *Phys. Rev. B*, 1994, **50**, 17953.

9 S. Mukhopadhyay, J. Debgupta, C. Singh, A. Kar and S. K. Das, *Angew. Chem. Int. Ed.,* 2018, **57**, 1918-1923.

10 N.-Y. Huang, J.-Q. Shen, Z.-M. Ye, W.-X. Zhang, P.-Q. Liao and X.-M. Chen, *Chem Sci.,* 2019, **10**, 9859-9864.

11 L. Yan, B. Zhang, J. Zhu, Z. Liu, H. Zhang and Y. Li, *J. Mater. Chem. A*, 2019, **7**, 22453-22462.

12 X. Zhou, S. Guo, Q. Cai and S. Huang, *Nanoscale,* 2019, **1**, 3686-3692.

13 M. Chen, Y. Xie, J.-X. Wu, H Huang, J. Teng, D. Wang, Y. Fan, J.-J. Jiang, H.-P. Wang and C.-Y. Su *J. Mater. Chem. A*, 2019, **7**,10217-10224.

14 Y. Tan, M. Luo, P. Liu, C. Cheng, J. Han, K. Watanabe and M. Chen, *ACS Appl. Mater. Interfaces*, 2019, **11**, 3880−3888.

15 H. Kim, J. Park, I. Park, K. Jin, S. E. Jerng, S. H. Kim, K. T. Nam and K. Kang, *Nat. Commun.,* 2015, **6,** 4532. B. Zhang, Y. H. Lui, H. Ni and S. Hu, *Nano Energy,* 2017, **38**, 553-560.

16 B. Jiang, X. Fan, Q Dang, F Liao, Y. Li, H. Lin, Z. Kang and M. Shao, *Nano Energy,* 2020, **76,** 105079.

17 L. Liu, D. Zhang, D. Duan, Y. Li, Q. Yuan, L. Chen and S. Liu, *J. Mater. Chem. C*, 2020, **862**, 114031

18 Y. Sun, T. Zhang, X. Li, D. Liu, G. Liu, X. Zhang, X. Lyu, W. Cai and Y. Li, *ChemComm,* 2017, **53**, 13237-13240.

19 L. Cao, J. Cai, W. Deng, Y. Tan and Q. Xie, *Anal. Chem.*, 2020, **92**, 16267-16273.

20 E. A. Turhan, S. V. K. Nune, E. Ülker, U. Şahin, Y. Dede and F. Karadas, *Chem-Eur J,* 2018, **24**, 10372-10382.

21 N.-Y. Huang, J.-Q. Shen, Z.-M. Ye, W.-X. Zhang, P.-Q. Liao and X.-M. Chen, *Chem Sci,* 2019, **10**, 9859-9864.

22 L. Ma, S.-F. Hung, L. Zhang, W. Cai, H. B. Yang, H. M. Chen and B. Liu, *Ind. Eng. Chem. Res.,* 2018, **57**, 1441-1445.

23 H. Wan, R. Ma, X. Liu, J. Pan, H. Wang, S. Liang, G. Qiu and T. Sasaki, *ACS Energy Lett.,* 2018, **3**, 1254-1260.

24 Z.-M. Luo, J.-W. Wang, J.-B. Tan, Z.-M. Zhang and T.-B. Lu, *ACS Appl. Mater. Interfaces,* 2018, **10**, 8231-8237.